Article:
Sun, N.-C., Maund, J.R. and Crowther, P.A. (2023) A UV census of the environments of stripped-envelope supernovae. Monthly Notices of the Royal Astronomical Society, 521 (2). pp. 2860-2873. ISSN: 0035-8711

https://doi.org/10.1093/mnras/stad690

Monthly Notices of the ROYAL ASTRONOMICAL SOCIETY

MNRAS **521,** 2860–2873 (2023) https://doi.org/10.1093/mnras/stad690
Advance Access publication 2023 March 7

A UV census of the environments of stripped-envelope supernovae

Ning-Chen Sun,[1,2,3]★ Justyn R. Maund[3] and Paul A. Crowther[3]

[1]*School of Astronomy and Space Science, University of Chinese Academy of Sciences, 19A Yuquan Road, Shijingshan District, Beijing 100049, China*
[2]*National Astronomical Observatories, Chinese Academy of Sciences, 20A Datun Road, Chaoyang District, Beijing 100101, China*
[3]*Department of Physics and Astronomy, University of Sheffield, Hicks Building, Hounsfield Road, Sheffield S3 7RH, UK*

Accepted 2023 March 1. Received 2023 February 7; in original form 2022 September 12

ABSTRACT

This paper reports an environmental analysis of 41 uniformly selected stripped-envelope supernovae (SESNe) based on deep ultraviolet–optical images acquired by the *Hubble Space Telescope*. Young stellar populations are detected in most SN environments and their ages are derived with a hierarchical Bayesian approach. The age distributions are indistinguishable between Type IIb and Type Ib, while that for Type Ic is systematically younger. This suggests that the Type Ic SN progenitors are more massive, while the Type IIb and Type Ib SNe have very similar progenitor masses. Our result supports a hybrid envelope-stripping mechanism, in which the hydrogen envelopes of the SESN progenitors are stripped via a mass-insensitive process (e.g. binary interaction), while the helium envelopes are stripped via a mass-sensitive process (e.g. stellar wind of the post-binary interaction progenitor). We also provide progenitor constraints for three Type Ibn SNe and two broad-lined Type Ic SNe. All these results demonstrate the importance of the very diverse mass-loss processes in the origins of SESNe.

Key words: supernovae: general – stars: mass-loss.

1 INTRODUCTION

Core-collapse supernovae (SNe) are the spectacular explosions of massive (>8 M$_\odot$) stars at the end of their lives. They disperse heavy elements from stars into the space, drive powerful feedback to the interstellar medium, and are associated with the formation of neutron stars or black holes (Heger et al. 2003). They are also important phenomena in multimessenger astronomy as possible sources of neutrinos, cosmic rays, and gravitational waves (Richardson et al. 2022).

The observational appearances of SNe are significantly affected by the various mass-loss processes of their progenitors. Single stars of $M_{\rm ini} = 8$–16 M$_\odot$ have relatively weak mass-loss and will finally explode as the hydrogen-rich Type II-P SNe (Smartt 2009). If a star's outer envelope is removed by a strong wind [for Wolf–Rayet (WR) stars with $M_{\rm ini} > 25$–30 M$_\odot$; Crowther 2007] and/or binary interaction (Podsiadlowski, Joss & Hsu 1992), the SN explosion will be of Type IIb (hydrogen lines visible only at early times), Ib (no hydrogen), or Ic (no hydrogen/helium). Some of the Type Ic SNe, referred to as the 'broad-lined' Type Ic (Ic-BL[1]) SNe or 'hypernovae', show very broad lines in their spectra owing to their extremely high explosion energies (Taddia et al. 2019). For some SNe, dense circumstellar material (CSM) can be formed if their progenitors undergo eruptive mass-loss shortly before explosion; the later ejecta–CSM interaction can produce strong and narrow emission lines, and such an SN will be of Type IIn, Ibn, or Icn depending on the chemical composition of the progenitor and its CSM (Smith 2014, 2017).

Arising from stripped progenitors, the hydrogen-poor SNe are also referred to as the 'stripped-envelope' (SE) SNe, including the above-mentioned types IIb, Ib, Ic, Ic-BL, Ibn, and Icn. Compared with the Type II-P SNe, the search for SESN progenitors on pre-explosion images has proven to be much more difficult. Currently, the progenitors have only been detected for five Type IIb SNe (1993J, 2008ax, 2011dh, 2013df, and 2016gkg; Aldering, Humphreys & Richmond 1994; Crockett et al. 2008; Maund et al. 2011; Van Dyk et al. 2014; Kilpatrick et al. 2017; Tartaglia et al. 2017), two Type Ib SNe (iPTF13bvn and 2019yvr; Cao et al. 2013; Eldridge et al. 2015; Kilpatrick et al. 2021; Sun et al. 2022), and one Type Ic SN (2017ein; Van Dyk et al. 2018; Xiang et al. 2019). Binary companions have (possibly) been detected for the Type IIb SN 1993J (Maund et al. 2004), SN 2001ig (Ryder et al. 2018), and SN 2011dh (Maund 2019), the Type Ib SN 2013ge (Fox et al. 2022) and SN 2019yvr (Sun et al. 2022), and the Type Ibn SN 2006jc (Maund et al. 2016; Sun et al. 2020a). In addition, host star clusters (which can be used to infer the progenitor properties) have been found for the Type Ib SN 2014C (Milisavljevic et al. 2015; Sun, Maund & Crowther 2020b) and the Type Ic SN 2020oi (Gagliano et al. 2022).

The limited number of these direct detections poses a major challenge to our understanding of the progenitors of SESNe and their pre-SN mass-loss. This motivates astronomers to explore alternative methods to constrain the progenitors for SESNe, such as measuring the line strengths of heavy elements in the nebular-phase spectra (e.g. Fang et al. 2019, 2022) and deriving the ejecta masses by fitting light curves (e.g. Lyman et al. 2016; Taddia et al. 2019). Environmental analysis is another powerful method to study SN progenitors, since most massive stars form in groups and stars in each group share very similar ages and metallicities (e.g. Anderson et al. 2012; Kangas et al. 2013; Galbany et al. 2018; Kuncarayakti et al. 2018; Schady et al. 2019; Xiao et al. 2019). Generally speaking, SNe from higher

★ E-mail: sunnc@ucas.ac.cn

[1]In the following, we shall use 'Type Ic' to refer to the normal ones, not including Type Ic-BL unless otherwise specified.

mass progenitors will more likely to be associated with tracers of recent star formation (e.g. Hα emission, dust, young stars, etc.), while those from lower mass progenitors may reside in much older environments.

Among the various techniques of environmental analysis, deep and high-spatial resolution imaging conducted by the *Hubble Space Telescope* (*HST*) can directly probe the stellar populations in the SN environments, and the stellar ages can be derived by fitting stellar isochrones on the colour–magnitude diagrams (CMDs; e.g. Maund & Ramirez-Ruiz 2016; Maund 2017, 2018; Williams et al. 2019; Sun et al. 2021, 2022). Compared with other techniques, this approach provides (relatively) more accurate age measurements. The past works have, however, largely relied on heterogeneous collections of archival observations and could suffer from statistical biases that are difficult to assess. Moreover, the age dependence of the colours of the very young and massive stars, often seen in SESN environments, is most sensitive at ultraviolet (UV) wavelengths. For many SESNe, however, observations have been performed only at optical wavelengths.

In this paper, we report a homogeneous set of deep UV–optical imaging observations of a uniformly selected sample of 41 SESNe in the Local Universe. Taking advantage of the UV filter and the deep detection limits, we try to probe the very young stellar populations in their environments and acquire an accurate determination of their ages. We also make statistical comparisons between the different SN types. Our aim is to reveal their possible progenitor channels and the roles of the various mass-loss processes in their origins.

This paper is structured as follows: In Section 2, we describe the sample selection, observation, photometry, and analysis; Section 3 provides the results and discussions for each individual SN type; and we finally close the paper with a summary and our conclusions in Section 4.

2 SAMPLE AND ANALYSIS

2.1 Target selection and observations

We selected Type IIb, Ib, and Ic SNe from the International Astronomical Union (IAU) SN list,[2] which occurred no earlier than the year of 1990, for the *HST* Snapshot programme '*A UV census of the sites of core-collapse SNe*' (PI: J. Maund; ID: 14762). The SNe were required to have a named host galaxy whose recession velocity corresponds to a Hubble-Flow distance of $\leq$25 Mpc (from the HyperLEDA data base[3] and corrected for the infall towards Virgo; Makarov et al. 2014). Only nine SNe were excluded from the selection since they already had deep UV observations in the *HST* archive. Besides, we added some important SNe (which had been heavily observed as part of photometric and spectroscopic campaigns) to our sample with higher priority and relaxed distance constraints, such as the Type Ibn and Type Ic-BL SNe. This strategy ensures that the targets were selected in a uniform and unbiased way with a good coverage of SN types.

44 SNe were finally observed by the *HST* from 2016 November to 2018 May with the UV–visible channel of the Wide Field Camera 3. The extremely wide UV filter *F*300*X* and optical filter *F*475*X* were used, with exposure times of 1200 and 350 s, respectively, for each target. Observations in each filter were divided into two individual exposures with a two-point dithering. The limiting magnitudes were typically 25.7 mag in *F*300*X* and 26.6 mag in *F*475*X* (magnitudes are reported in the Vega system throughout this paper). The choice of the extremely wide filter *F*300*X* and the long exposure times ensure that the young stellar populations can be probed down to very deep limits.

Out of the observed SNe, we later found that SN 2006oz is actually a superluminous SN in a very distant dwarf galaxy (Leloudas et al. 2012) and SN 2008ha is a peculiar Type Iax SN whose nature is not yet clear (Foley et al. 2009); these two SNe were excluded in this work. SN 2005ar was also excluded since it is located at more than 100 Mpc away according to more recent distance measurements. The remaining 41 SESNe, listed in Table 1, were finally used for the following analysis, including 13 IIb, 9 Ib, 10 Ic, 4 intermediate or ambiguous Ib/Ic, 3 Ibn, and 2 Ic-BL.

Table 1 also provides the Galactic extinctions and the host galaxy inclinations and distances. Galactic extinctions are based on the estimates by Schlafly & Finkbeiner (2011) and obtained from the NASA/IPAC IRSA Dust Extinction Service.[4] Host galaxy inclinations are from the HyperLEDA data base. Distances to the SN host galaxies, when possible, are from the CosmicFlows project[5] (Tully et al. 2013; Tully, Courtois & Sorce 2016); for the other galaxies, we use Hubble-Flow distances adopting a Hubble constant of $H_0 = 73.0 \pm 5$ km s^{-1} Mpc^{-1}. Note that, although we aimed to select targets within 25 Mpc based on their recession velocities, some of the observed SNe have larger distances according to the more accurate CosmicFlows project.

We have not included any SESNe with archival *HST* data in order to ensure the uniformity in source selection and observations. The archival data are from various observing programmes with different source selection criteria; therefore, including them would introduce some non-uniformity that itself is complicated and difficult to assess. For example, if the archival observations were aimed at studying active galactic nuclei, the SNe within the images would appear in the inner parts of the galaxies and those in the outer parts may fall outside the fields of view. In addition, the archival data had a range of filters, predominantly in the optical (there were only nine SNe observed in the UV before this programme, although the number has increased recently). By sticking with the extremely wide *F*300*X* and *F*475*X* filters (to obtain high throughputs, which are rarely used by other observations) and the same exposure times for all targets, we try to acquire a uniform set of observations.

2.2 Image processing and photometry

Images processed by the standard reduction pipeline (`*_flc.fits` and `*_drc.fts`) were retrieved from the Mikulski Archive for Space Telescopes.[6] The images still contain a high level of cosmic ray residuals; therefore, we redrizzled them with `driz_cr_grow = 3` with the ASTRODRIZZLE package,[7] which can clean the cosmic rays much more efficiently (all other parameters were unchanged).

We performed photometry with the DOLPHOT package (Dolphin 2000) by fitting model point spread functions (PSFs) to the sources. The DOLPHOT parameters `FitSky = 2` and `Img_RAper = 3` were used, which perform better in crowded regions. We turned off aperture corrections with `ApCor = 0` since some images have very few stars for this purpose, causing large uncertainties (note that typical aperture corrections are only about several hundredths of

[2] http://www.cbat.eps.harvard.edu/lists/Supernovae.html
[3] http://leda.univ-lyon1.fr
[4] https://irsa.ipac.caltech.edu/applications/DUST
[5] http://edd.ifa.hawaii.edu
[6] https://archive.stsci.edu/index.html
[7] http://drizzlepac.stsci.edu/

Table 1. Sample of SESNe analysed in this work.

Target	Type	Host galaxy	Distance D (Mpc)	Inclination θ (deg)	Galactic extinction $A_V^{\rm MW}$ (mag)	References
1996cb	IIb	NGC 3510	16.8 (2.3)	78.1	0.08	Qiu et al. (1999)
2003bg	IIb	ESO 420-g009	17.7 (1.2)	41.7	0.06	Hamuy et al. (2009), Mazzali et al. (2009)
2004C	IIb	NGC 3683	32.1 (4.4)	69.0	0.04	Shivvers et al. (2017a)
2005ae	IIb	ESO 209-g9	13.6 (1.9)	90.0	0.69	Filippenko & Foley (2005)
2008bo	IIb	NGC 6643	20.9 (2.9)	62.7	0.16	Navasardyan et al. (2008)
2009dq	IIb	IC 2554	16.4 (1.1)	70.8	0.55	Green (2009a)
2009gj	IIb	NGC 134	19.2 (2.7)	90.0	0.05	Foley (2009)
2009mk	IIb	ESO 293-g34	20.7 (1.4)	74.6	0.04	Chornock & Berger (2009)
2010as	IIb	NGC 6000	31.0 (2.1)	30.7	0.46	Folatelli et al. (2014)
2011hs	IIb	IC 5267	20.9 (4.8)	47.8	0.03	Milisavljevic et al. (2011)
2013df	IIb	NGC 4414	17.9 (1.4)	56.6	0.05	Van Dyk et al. (2014)
2015Y	IIb	NGC 2735	54.7 (11.3)	74.2	0.10	Childress et al. (2015)
2016bas	IIb	ESO 163-g11	50.6 (9.3)	70.9	0.40	Hosseinzadeh et al. (2016a)
1996N	Ib	NGC 1398	28.6 (5.9)	47.5	0.04	Sollerman, Leibundgut & Spyromilio (1998)
2000ds	Ib	NGC 2768	22.2 (2.9)	90.0	0.12	Filippenko & Chornock (2000)
2001B	Ib	IC 391	25.2 (1.7)	18.1	0.34	Chornock & Filippenko (2001)
2004ao	Ib	UGC 10862	29.6 (2.0)	53.4	0.27	Matheson et al. (2004b)
iPTF13bvn	Ib	NGC 5806	27.0 (3.7)	60.4	0.14	Cao et al. (2013)
2014C	Ib	NGC 7331	14.1 (1.0)	70.0	0.24	Kim et al. (2014), Milisavljevic et al. (2015)
2014df	Ib	NGC 1448	17.2 (1.3)	86.4	0.04	Monard et al. (2014)
2015Q	Ib	NGC 3888	39.3 (2.7)	36.3	0.03	Wiggins et al. (2015)
2016cdd	Ib	ESO 218-g8	28.7 (2.0)	90.0	0.49	Hosseinzadeh et al. (2016b)
1990W	Ic	NGC 6221	11.9 (1.6)	50.9	0.44	della Valle et al. (1990), Filippenko & McCarthy (1990)
2000ew	Ic	NGC 3810	15.9 (2.2)	48.2	0.12	Filippenko, Chornock & Modjaz (2000)
2001ci	Ic	NGC 3079	20.6 (3.8)	90.0	0.03	Filippenko & Chornock (2001)
2004bm	Ic	NGC 3437	24.2 (3.3)	72.8	0.05	Foley et al. (2004)
2004gk	Ic	IC 3311	20.6 (2.8)	90.0	0.08	Quimby et al. (2004)
2005at	Ic	NGC 6744	9.0 (0.7)	53.5	0.11	Kankare et al. (2014), Schmidt & Salvo (2005)
2005aw	Ic	IC 4837a	41.6 (2.9)	90.0	0.16	Morrell et al. (2005)
2009em	Ic	NGC 157	12.1 (2.2)	61.8	0.12	Green (2009b), Navasardyan & Benetti (2009)
2012cw	Ic	NGC 3166	22.0 (1.5)	56.2	0.08	Itagaki et al. (2012)
2012fh	Ic	NGC 3344	9.8 (0.9)	18.7	0.09	Nakano et al. (2012)
1991N	Ib/Ic	NGC 3310	19.2 (1.3)	16.1	0.06	Filippenko & Korth (1991)
1995F	Ib/Ic	NGC 2726	55.7 (10.3)	90.0	0.10	Lane et al. (1995)
2005V	Ib/Ic	NGC 2146	16.7 (1.2)	37.4	0.26	Beswick et al. (2005), Taubenberger et al. (2005)
2013ge	Ib/Ic	NGC 3287	14.6 (2.0)	75.3	0.06	Drout et al. (2016)
2006jc	Ibn	UGC 4904	27.8 (1.9)	52.2	0.05	Foley et al. (2007), Pastorello et al. (2007)
2015G	Ibn	NGC 6951	18.8 (1.7)	50.8	0.99	Shivvers et al. (2017b)
2015U	Ibn	NGC 2388	60.3 (11.1)	52.6	0.15	Shivvers et al. (2016)
1997dq	Ic-BL	NGC 3810	15.9 (2.2)	48.2	0.12	Mazzali et al. (2004)
2002ap	Ic-BL	NGC 628	9.8 (0.9)	19.8	0.19	Kinugasa et al. (2002)

magnitude, which is much smaller than the random errors). `Force1 = 1` was used for better modelling of close stars that may be blended with each other. All other parameters were the same as those recommended in the DOLPHOT user manual.[8]

A detection reported by DOLPHOT is considered to be a good star if its quality parameters meet the following criteria:

(1) type of source, TYPE = 1;
(2) signal-to-noise ratio, SNR $\geq$ 5;
(3) source sharpness, $-0.5 \leq$ SHARP ≤ 0.5;
(4) source crowding, CROWD ≤ 2;
(5) photometry quality flag, FLAG ≤ 3.

For stars detected in only one filter, we used artificial stars, inserted at each source position, to estimate the detection limit in the other filter. An artificial star was considered to be successfully recovered if it fell within 1 pixel of the inserted position and its DOLPHOT quality parameters met all the above criteria. The detection limits were derived independently for each star since the sky background and source crowding may vary across the field. We also used randomly positioned artificial stars to estimate additional photometric uncertainties induced by source crowding and imperfect sky subtraction.

We determined SN positions on the *HST* images with three different methods depending on the availability of supporting observations: (1) relative astrometry with previous *HST* observations, with typical uncertainties of <1 pixel; (2) relative astrometry with observations from other telescopes (e.g. *Swift*/UVOT and *Spitzer*/IRAC), with typical uncertainties of $\sim$3 pixel; and (3) using the reported SN RA and Dec. coordinates, with typical uncertainties of $\sim$1 arcsec. Sources within a (projected) distance of 150 pc from the SN positions (excluding those within 3 pixels from the SNe) were finally selected for the

[8] http://americano.dolphinsim.com/dolphot/dolphotWFC3.pdf

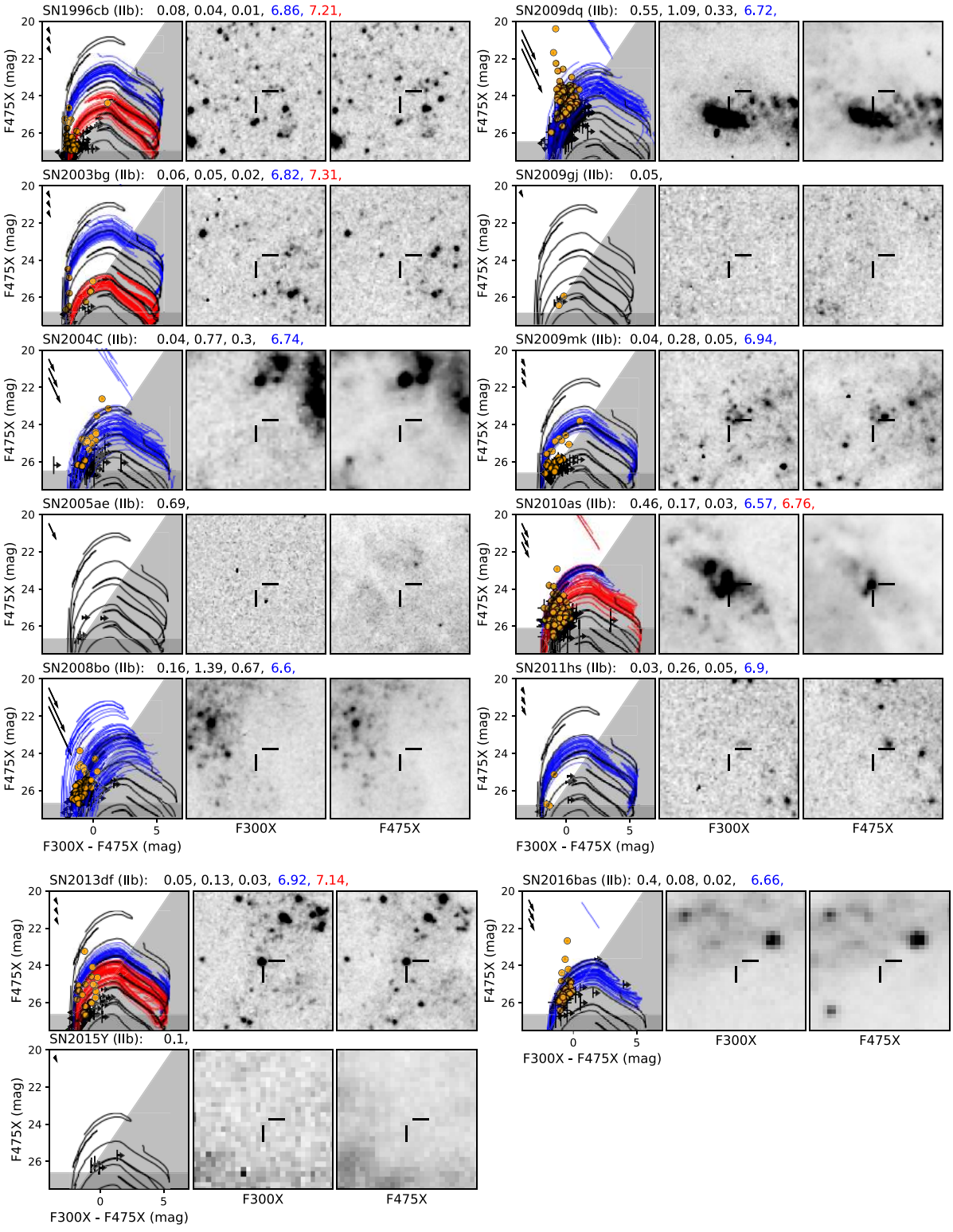

Figure 1. CMDs and *HST* images of the Type IIb SN environments as listed in Table 1. The *HST* images have sizes of 300 pc × 300 pc and are centred on the SN positions (indicated by the crosshairs). The circular region we defined for environmental analysis has a radius of 150 pc, i.e. a diameter equal to the box size. In the CMDs, the grey-shaded regions show the average detection limits for a random position in the SN environments, below which the 5σ detection probability falls below 50 per cent. Overlaid are PARSEC (v1.2S) stellar isochrones; the coloured ones correspond to the fitted model stellar populations, with blue, red, and green colours used for populations of increasing ages, and, for each age component, we show 30 random realizations derived from their age and extinction spreads; for reference, we also show black isochrones with log ages of 6.6, 6.8, 7.0, ... in equal spacing of 0.2 dex, all reddened with the Galactic and mean internal extinction. The title for each SN lists the values of Galactic extinction $A_V^{\rm MW}$, and if a stellar population fitting is performed, the mean internal extinction $A_V^{\rm int}$, internal extinction standard deviation $\mathrm{d}A_V^{\rm int}$, and mean log ages of the model stellar populations $\log(t_i/\mathrm{yr})$ ($i = 1$, 2, and 3). The three arrows in the upper left corners show the reddening vectors with lengths corresponding to $A_V^{\rm MW} + A_V^{\rm int}$ ($\pm\mathrm{d}A_V^{\rm int}$).

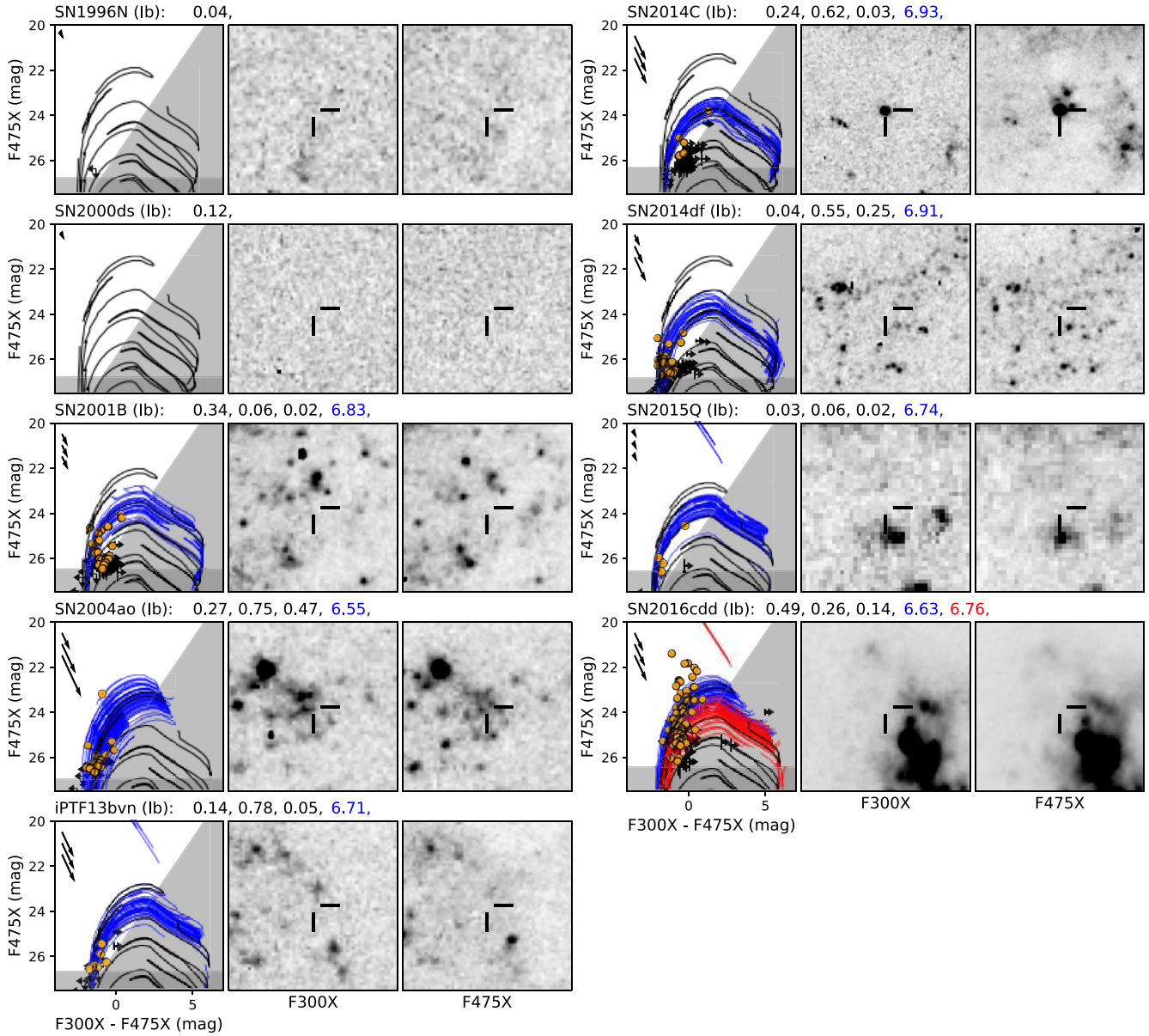

Figure 2. Same as Fig. 1 but for Type Ib SNe.

following analysis (we did not correct for the host galaxies' inclinations). Consistent with the previous studies (e.g. Maund 2017, 2018), the size of the selection region was chosen to be compatible with the typical scales of star-forming complexes, i.e. fundamental cells of star formation within which the stars are born with similar ages (Efremov 1995). The SN positional errors are not important compared with the defined area. Figs 1–6 show the images of the observed SN sites and the CMDs of the detected sources in their environments.

2.3 Fitting of the resolved stellar populations

2.3.1 Method

In order to derive the stellar ages, we used a hierarchical Bayesian approach to fit model stellar populations to the observed stars in the SN environments. The method is described in detail in Maund & Ramirez-Ruiz (2016) and Sun et al. (2021) and has been successfully applied in a number of studies (e.g. Maund 2017, 2018; Sun et al. 2020a, 2021, 2022). In brief, the model populations were simulated based on the PARSEC stellar isochrones (v1.2S; Bressan et al. 2012) and have a Salpeter (1955) initial mass function, a 50 per cent binary fraction, and a flat distribution of primary-to-secondary mass ratio. In addition to the Galactic extinction, the internal extinctions from the host galaxy were assumed to have a Gaussian distribution $\mathcal{N}(A_V^{\rm int}, ({\rm d}A_V^{\rm int})^2)$ among the stars in each SN environment, where $A_V^{\rm int}$ is the mean value and ${\rm d}A_V^{\rm int}$ is the standard deviation; we used a flat prior for $A_V^{\rm int}$ and a logarithmic prior for ${\rm d}A_V^{\rm int}$ over the range of $0 \leq \log({\rm d}A_V^{\rm int}/0.01\ {\rm mag}) \leq 2$, penalizing large values. In each SN environment, the observed stars can be considered as arising from a mixture of model stellar populations with different ages and each model population corresponds to a short burst of star formation, in which the stellar log ages follow a narrow Gaussian distribution with a standard deviation of 0.05 dex.

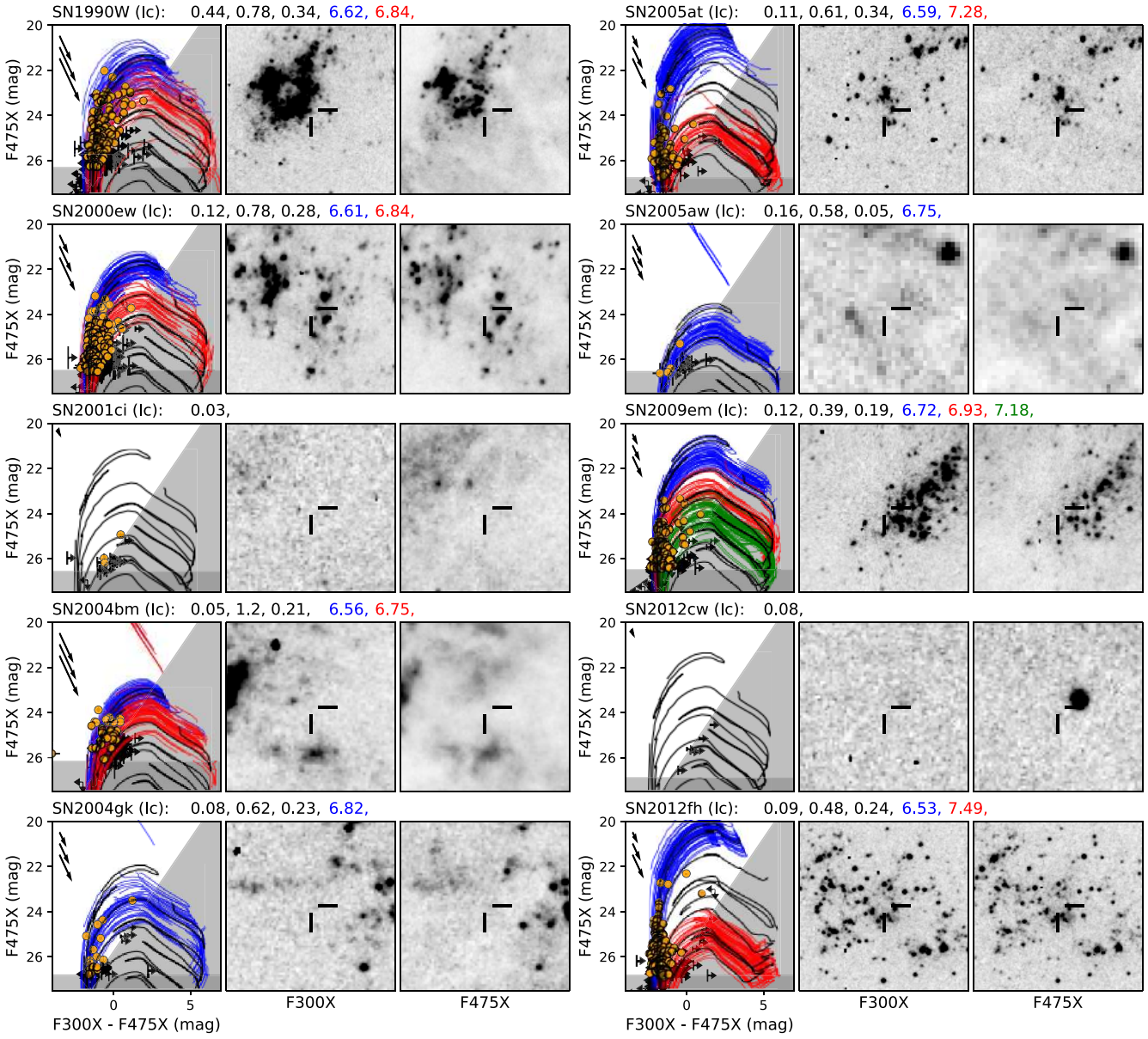

Figure 3. Same as Fig. 1 but for Type Ic SNe.

To determine the required number of model populations, we started the fitting with one age component, and added more age components if the fitting was significantly improved. We compared the fitting performances using the Bayes factor $K_{n+1,n} = [Z_{n+1}/(n + 1)!]/(Z_n/n!)$ and the criterion of Jeffreys (1961), where Z_{n+1} and Z_n are the Bayesian pieces of evidence for the fitting with $n + 1$ and n components [note that factors of $n!$ and $(n + 1)!$ are needed to correct for overestimation since the labels for the model populations are interchangeable with each other]. We stopped adding more components if this did not improve the fitting significantly or if the number of components reached a maximum value of 3. In practice, all SNe, except the Type Ic SN 2009em, require fewer than three age components to model the detected populations.

We did not perform any fitting when the SN environments contain no stars detected in both filters or only a few stars marginally detected above the detection limits. For each SN environment, we also estimated an age limit older than which a stellar population will fall below the detection limits; in doing this, we use the same extinction as derived from the population fitting, or simply assume zero internal extinction if no population fitting is performed for the SN (but this may overestimate the age limit).

2.3.2 *Caveats*

At the distances of the analysed SNe, the linear size of a pixel corresponds to a few parsecs and the detected sources may or may not be single stars. In our population modelling, we have considered the possibilities of each source being a non-interacting binary system [Section 2.3.1; see also Maund & Ramirez-Ruiz (2016) and Sun et al. (2021) for details], for which the composite fluxes are the simple sums of the primary and secondary stars' fluxes. This approach also accounts for the visual binaries composed of stars in chance alignment; thus, source blending in crowded regions does not have a significant influence on our results (the visual binaries slightly

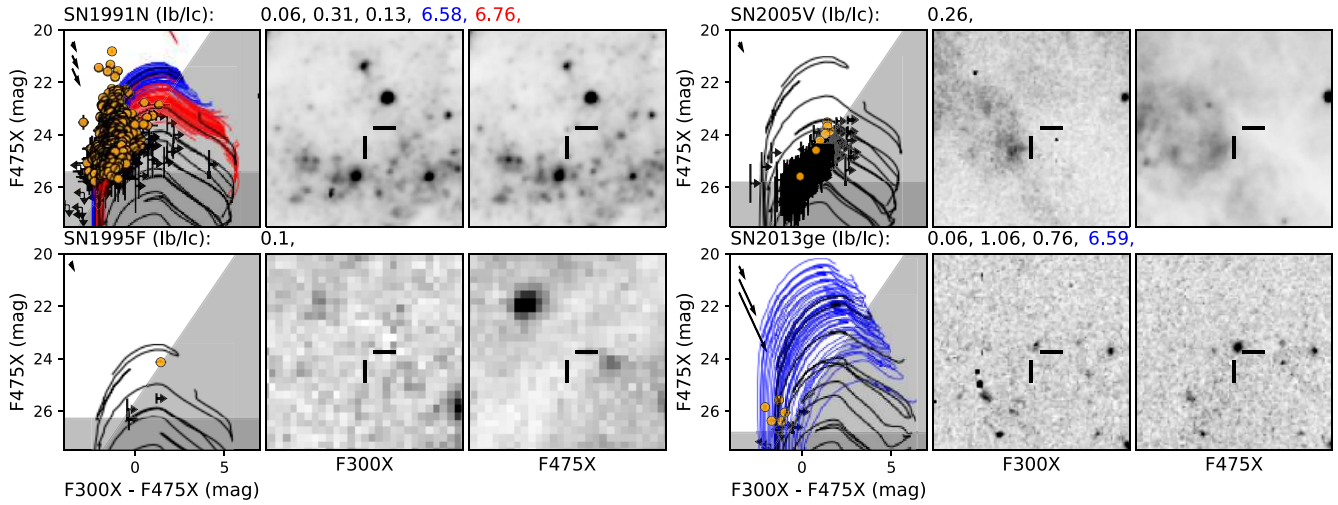

Figure 4. Same as Fig. 1 but for intermediate or ambiguous Type Ib/Ic SNe.

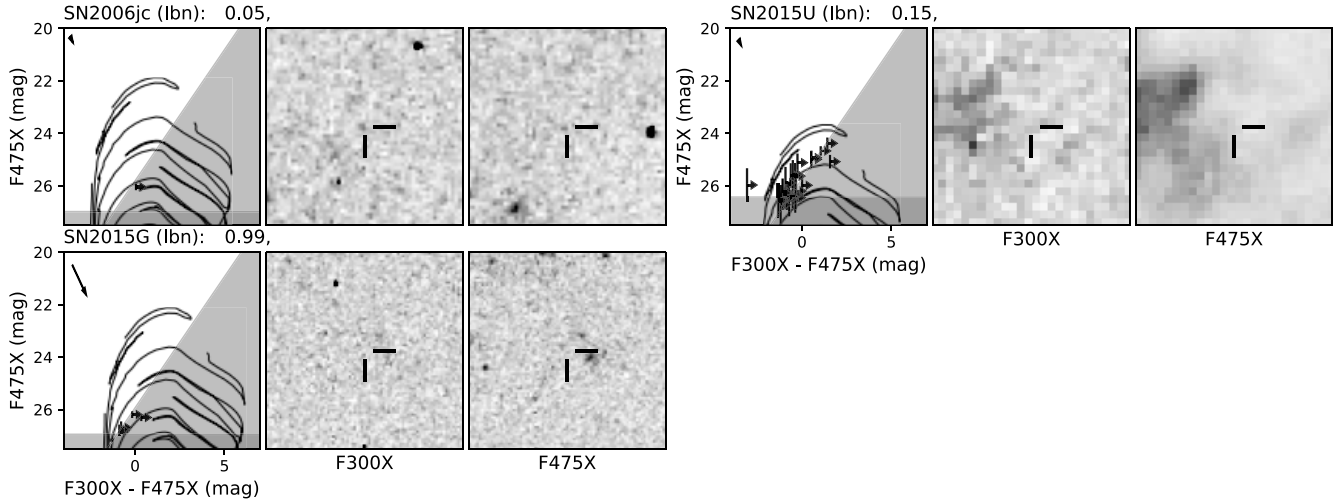

Figure 5. Same as Fig. 1 but for Type Ibn SNe.

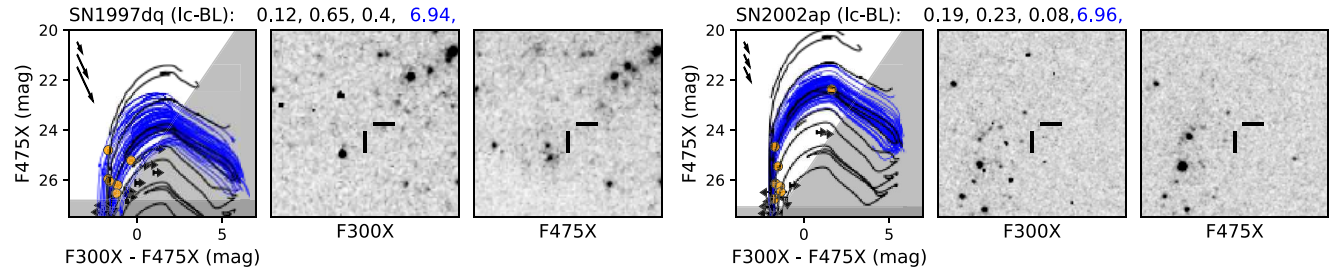

Figure 6. Same as Fig. 1 but for Type Ic-BL SNe.

increase the effective binary fraction, to which the population fitting is not very sensitive). However, this effect may still lead to an age underestimation in particular if the source lies in a region on the CMD where stars evolve very rapidly (and thus drives the fitting most sensitively). We have not considered the contribution from interacting binaries. The rejuvenated stars from binary mass transfer and merger may appear much younger (Schneider et al. 2015); therefore, our analysis tends to underestimate the stellar ages. It is, however, not trivial to model the interacting binary populations; this requires a detailed binary population synthesis and is beyond the scope of this work.

Star clusters that appear more extended than the PSF have been excluded by the selection criteria in Section 2.2 (extended sources have low sharpness values reported by DOLPHOT). We cannot rule out the possibility that the stellar catalogues are still contaminated by very compact star clusters that are not spatially resolved due to their small angular sizes. In some SN environments, some sources appear much brighter than the other sources and are more likely to

Table 2. Parameters derived from the stellar population fitting for the SN environments. $N_{\rm m}$: number of age components to fit the observed stars; $A_V^{\rm int}$ and ${\rm d}A_V^{\rm int}$: the mean value and standard deviation of the internal extinctions from the host galaxy, respectively; $\log(t_i/{\rm yr})$ and w_i ($i = 1, 2, 3$): mean stellar log age and weight for the i-th age component; $\log(t_{\rm lim}/{\rm yr})$: age limit older than which a stellar population will fall below the detection limits. The last column gives the numbers of data points used in the fitting, with $N_{\rm both}$, N_{F300X}, and N_{F475X} corresponding to those detected in both bands, only in the *F*300*X* band, and only in the *F*475*X* band, respectively. The errors are propagated from photometric uncertainties.

Target	Type	$N_{\rm m}$	$A_V^{\rm int}$ (mag)	${\rm d}A_V^{\rm int}$ (mag)	$\log(t_1/{\rm yr})$	w_1	$\log(t_2/{\rm yr})$	w_2	$\log(t_3/{\rm yr})$	w_3	$\log(t_{\rm lim}/{\rm yr})$	$N_{\rm both}, N_{F300X}, N_{F475X}$
1996cb	IIb	2	$0.04^{+0.02}_{-0.01}$	$0.01^{+0.01}_{-0.00}$	$6.86^{+0.03}_{-0.03}$	0.64	$7.21^{+0.03}_{-0.03}$	0.36	...	...	7.5	25, 23, 16
2003bg	IIb	2	$0.05^{+0.03}_{-0.02}$	$0.02^{+0.01}_{-0.00}$	$6.82^{+0.04}_{-0.08}$	0.72	$7.31^{+0.12}_{-0.11}$	0.28	...	...	7.5	10, 10, 5
2004C	IIb	1	$0.77^{+0.11}_{-0.12}$	$0.30^{+0.06}_{-0.07}$	$6.74^{+0.02}_{-0.02}$	1.00	...	...	...	...	6.9	17, 2, 37
2005ae	IIb	0	...	...	...	...	...	...	...	...	7.3	–
2008bo	IIb	1	$1.39^{+0.09}_{-0.09}$	$0.67^{+0.06}_{-0.06}$	$6.60^{+0.03}_{-0.02}$	1.00	...	...	...	...	6.8	43, 12, 38
2009dq	IIb	1	$1.09^{+0.05}_{-0.05}$	$0.33^{+0.03}_{-0.03}$	$6.72^{+0.01}_{-0.01}$	1.00	...	...	...	...	6.9	74, 5, 195
2009gj	IIb	0	...	...	...	...	...	...	...	...	7.5	–
2009mk	IIb	1	$0.28^{+0.06}_{-0.06}$	$0.05^{+0.03}_{-0.05}$	$6.94^{+0.02}_{-0.02}$	1.00	...	...	...	...	7.3	22, 8, 21
2010as	IIb	2	$0.17^{+0.10}_{-0.07}$	$0.03^{+0.03}_{-0.02}$	$6.57^{+0.03}_{-0.03}$	0.38	$6.76^{+0.01}_{-0.01}$	0.62	...	...	7.0	56, 5, 52
2011hs	IIb	1	$0.26^{+0.14}_{-0.12}$	$0.05^{+0.06}_{-0.05}$	$6.90^{+0.12}_{-0.06}$	1.00	...	...	...	...	7.4	3, 1, 4
2013df	IIb	2	$0.13^{+0.05}_{-0.04}$	$0.03^{+0.02}_{-0.02}$	$6.92^{+0.02}_{-0.02}$	0.62	$7.14^{+0.04}_{-0.04}$	0.38	...	...	7.4	19, 24, 19
2015Y	IIb	0	...	...	...	...	...	...	...	...	7.0	–
2016bas	IIb	1	$0.08^{+0.04}_{-0.03}$	$0.02^{+0.01}_{-0.01}$	$6.66^{+0.01}_{-0.01}$	1.00	...	...	...	...	6.8	25, 1, 13
1996N	Ib	0	...	...	...	...	...	...	...	...	7.3	–
2000ds	Ib	0	...	...	...	...	...	...	...	...	7.4	–
2001B	Ib	1	$0.06^{+0.03}_{-0.02}$	$0.02^{+0.01}_{-0.00}$	$6.83^{+0.01}_{-0.01}$	1.00	...	...	...	...	7.2	28, 8, 23
2004ao	Ib	1	$0.75^{+0.11}_{-0.11}$	$0.47^{+0.08}_{-0.08}$	$6.55^{+0.04}_{-0.04}$	1.00	...	...	...	...	6.9	19, 5, 6
iPTF13bvn	Ib	1	$0.78^{+0.13}_{-0.13}$	$0.05^{+0.06}_{-0.05}$	$6.71^{+0.04}_{-0.04}$	1.00	...	...	...	...	7.0	6, 0, 2
2014C	Ib	1	$0.62^{+0.04}_{-0.04}$	$0.03^{+0.03}_{-0.03}$	$6.93^{+0.01}_{-0.01}$	1.00	...	...	...	...	7.3	5, 3, 40
2014df	Ib	1	$0.55^{+0.06}_{-0.06}$	$0.25^{+0.04}_{-0.05}$	$6.91^{+0.02}_{-0.02}$	1.00	...	...	...	...	7.3	21, 14, 21
2015Q	Ib	1	$0.06^{+0.07}_{-0.04}$	$0.02^{+0.02}_{-0.01}$	$6.74^{+0.03}_{-0.03}$	1.00	...	...	...	...	7.1	4, 2, 1
2016cdd	Ib	2	$0.26^{+0.04}_{-0.04}$	$0.14^{+0.03}_{-0.03}$	$6.63^{+0.01}_{-0.01}$	0.75	$6.76^{+0.02}_{-0.03}$	0.25	...	...	6.9	65, 7, 22
1990W	Ic	2	$0.78^{+0.04}_{-0.04}$	$0.34^{+0.03}_{-0.03}$	$6.62^{+0.01}_{-0.02}$	0.68	$6.84^{+0.02}_{-0.02}$	0.32	...	...	7.2	176, 32, 60
2000ew	Ic	2	$0.78^{+0.06}_{-0.07}$	$0.28^{+0.04}_{-0.05}$	$6.61^{+0.03}_{-0.02}$	0.50	$6.84^{+0.01}_{-0.01}$	0.50	...	...	7.2	128, 21, 57
2001ci	Ic	0	...	...	...	...	...	...	...	...	7.4	–
2004bm	Ic	2	$1.20^{+0.05}_{-0.06}$	$0.21^{+0.05}_{-0.07}$	$6.56^{+0.03}_{-0.03}$	0.25	$6.75^{+0.01}_{-0.01}$	0.75	...	...	6.9	34, 2, 76
2004gk	Ic	1	$0.62^{+0.12}_{-0.16}$	$0.23^{+0.07}_{-0.12}$	$6.82^{+0.04}_{-0.03}$	1.00	...	...	...	...	7.2	16, 8, 13
2005at	Ic	2	$0.61^{+0.07}_{-0.07}$	$0.34^{+0.05}_{-0.05}$	$6.59^{+0.10}_{-0.11}$	0.76	$7.28^{+0.05}_{-0.07}$	0.24	...	...	7.6	57, 24, 13
2005aw	Ic	1	$0.58^{+0.12}_{-0.13}$	$0.05^{+0.06}_{-0.06}$	$6.75^{+0.02}_{-0.02}$	1.00	...	...	...	...	6.9	4, 0, 13
2009em	Ic	3	$0.39^{+0.04}_{-0.04}$	$0.19^{+0.03}_{-0.02}$	$6.72^{+0.03}_{-0.04}$	0.56	$6.93^{+0.04}_{-0.05}$	0.30	$7.18^{+0.05}_{-0.04}$	0.14	7.5	102, 37, 21
2012cw	Ic	0	...	...	...	...	...	...	...	...	7.4	–
2012fh	Ic	2	$0.48^{+0.03}_{-0.03}$	$0.24^{+0.02}_{-0.02}$	$6.53^{+0.05}_{-0.06}$	0.85	$7.49^{+0.04}_{-0.03}$	0.15	...	...	7.6	126, 39, 30
1991N	Ib/Ic	2	$0.31^{+0.03}_{-0.02}$	$0.13^{+0.01}_{-0.01}$	$6.58^{+0.01}_{-0.01}$	0.86	$6.76^{+0.01}_{-0.01}$	0.14	...	...	7.1	345, 35, 34
1995F	Ib/Ic	0	...	...	...	...	...	...	...	...	6.9	–
2005V	Ib/Ic	0	...	...	...	...	...	...	...	...	7.3	–
2013ge	Ib/Ic	1	$1.06^{+0.25}_{-0.26}$	$0.76^{+0.12}_{-0.17}$	$6.59^{+0.20}_{-0.22}$	1.00	...	...	...	...	7.2	5, 5, 4
2006jc	Ibn	0	...	...	...	...	...	...	...	...	7.3	–
2015G	Ibn	0	...	...	...	...	...	...	...	...	7.2	–
2015U	Ibn	0	...	...	...	...	...	...	...	...	6.9	–
1997dq	Ic-BL	1	$0.65^{+0.17}_{-0.16}$	$0.40^{+0.12}_{-0.13}$	$6.94^{+0.05}_{-0.05}$	1.00	...	...	...	...	7.3	6, 7, 9
2002ap	Ic-BL	1	$0.23^{+0.10}_{-0.07}$	$0.08^{+0.06}_{-0.10}$	$6.96^{+0.04}_{-0.05}$	1.00	...	...	...	...	7.6	7, 7, 2

be star clusters; they were manually removed from the fitting. For the ambiguous sources that are not easily identifiable by eye, our algorithm also automatically assigns lower weights to the 'outliers' in determining the model populations' parameters. For the low-mass star clusters whose brightnesses are often dominated by one or a few massive stars (e.g. the Orion Nebula Cluster), they can be fitted by our algorithm as if they are bright stars or binary systems. Proper quantitative assessment would require a detailed modelling of the star cluster population, which is beyond the scope of this work.

When available, we adopted metallicities for the model stellar populations that follow the reported values for the SNe. For those without metallicity estimates, we assume half-solar metallicity for the Type Ic-BL SNe (which prefer low-metallicity environments; Modjaz et al. 2020) and solar metallicity for the other types. We ignored the metallicity uncertainties/dispersions and fixed their values

in the fitting. This simplification greatly reduces the computing time. However, this may introduce some systematic errors since the stellar colours are metallicity dependent.

Distances are fixed in our stellar population fitting. The typical uncertainties in distance moduli are 0.15–0.40 dex with a median value of 0.2 dex. By manually fitting stellar isochrones while keeping the extinction unchanged, we found that a 0.2-dex difference in the distance modulus roughly corresponds to a difference of 0.03 dex in stellar log age. We also carried out a test by adding or subtracting 0.2 dex from the used distance modulus, and the derived ages changed by a negligible amount (in particular for the youngest population), since part of the distance difference has been absorbed by the internal extinction as a free parameter.

It was found that in some SN environments (e.g. SN 2004dg and SN 2012P; Sun et al. 2021) stars formed at different epochs may be located at different places along the line of sight and have different extinction values. For simplicity, however, our analysis assumes that $A_V^{\rm int}$ and $\mathrm{d}A_V^{\rm int}$ are independent of stellar ages. While this may introduce some systematic uncertainties, this simplification does not affect the youngest populations (which we shall focus on) that dominate the observed stars and drive the fitting in most circumstances. In the analysis, we have used a standard extinction law with $R_V = 3.1$ (Fitzpatrick 2004) for both the Galactic and internal extinctions. We repeated the fitting with different values of $R_V = 2.0$ and 5.0 for the internal extinction; although the derived extinctions may be different, the populations' ages change very little by <0.05 dex. Therefore, the reported ages are relatively insensitive to the choice of the reddening law. The fitting results are also unaffected by the uncertainties in the Galactic extinction, since any such errors will be absorbed by the internal extinction, which is a free parameter to be fitted.

We have not considered the stochastic sampling effect when the number of data points is very small. If the fitting is driven by only a few data points, the nominal uncertainty propagated from the photometric errors could be significantly underestimated. While it is difficult to make quantitative measurement, we caution this effect and provide the numbers of data points used in the fitting in the last column of Table 2.

Lastly, we have assumed zero uncertainty in the adopted stellar isochrones. However, the evolution for young and massive stars is not well constrained and different sets of models could predict different evolutionary tracks (Martins & Palacios 2013). The model uncertainty is another source of error in our results.

3 RESULTS AND DISCUSSIONS

The population fitting results are listed in Table 2 and also displayed in Fig. 7. The quoted uncertainties are propagated from the photometric errors and are estimated with the 68 per cent equal-tailed credible intervals (we also explore the effects of additional uncertainties in Section 3.1); therefore, the uncertainties become larger when there is a significant degeneracy between age and extinction with double-peaked posterior probability distributions. The results show that very young stellar populations are present in the environments of a large fraction of the SESNe. ∼80 per cent of the observed types IIb, Ib, and Ic SNe have stellar populations younger than 10 Myr in their vicinity (10/13 Type IIb, 7/9 Type Ib, 8/10 Type Ic, and 2/4 SNe that are of intermediate or ambiguous Type Ib/Ic) and this fraction may be even higher if some SN environments contain young stars from residual star formation that have eluded our detection. For the Type Ic SN 1997dq and SN 2002ap, young stellar populations are detected in their environments with ages of $\log(t/\mathrm{yr}) = 6.94$ and 6.96,

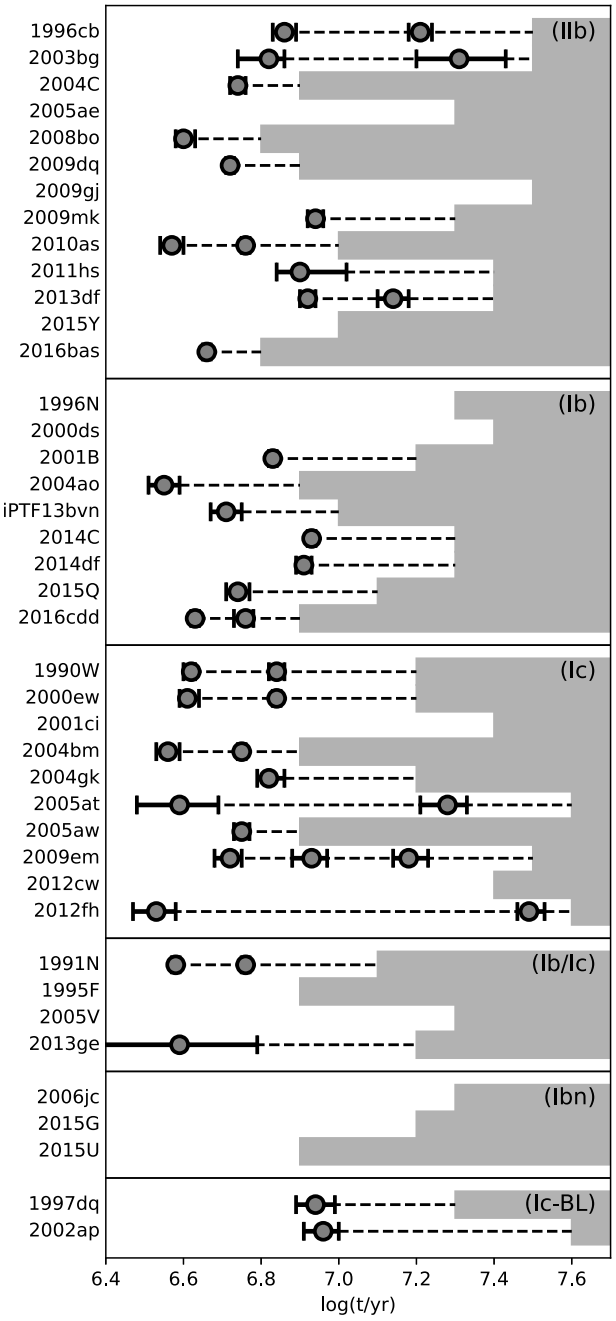

Figure 7. Ages of the resolved stellar populations in the SN environments. The shaded regions show the age limits older than which a stellar population will fall below the detection limits.

respectively. In contrast, the Type Ibn SN 2006jc and SN 2015G are located in very sparse areas without any obvious recent star formation, and SN 2015U does not have any resolved stars in its vicinity that are significantly detected in the UV filter.

It is worth noting that the age limits (older than which a stellar population will not be detected in both filters) are not the same for all targets and are strongly dependent on their distances and extinctions. Therefore, we shall characterize the age of each SN environment not with all the detected populations, but only with the youngest one, which is less affected by the inhomogeneous age limit.

The presence of very young stellar populations in the environment is often interpreted as the SNe having very massive progenitors

with similarly young ages (e.g. WR stars). However, it should be cautioned that the SN progenitors may actually be much older and reside just in chance alignment. Also note that star formation bursts on small scales may appear correlated if they are controlled by physical processes on larger scales (e.g. spiral density waves that sweep up and compress the upstream low-density gas and leave behind a trail of sequential star formation at the downstream, Sun et al. 2021; the feedback from massive stars that can trigger new episodes of star formation in their vicinity, Koenig et al. 2008; and the ubiquitous supersonic turbulence that drives hierarchical patterns in the spatial distribution of star formation, Sun et al. 2017a,b, 2018; Miller et al. 2022). The relationship between an SN progenitor and the youngest stellar population in its environment may therefore be very complicated: the progenitor may (1) be a member of the youngest population and have the same age, (2) form at an earlier epoch of star formation *unrelated* to the youngest population and aligned just by chance, or (3) arise from an older stellar population in the vicinity of the youngest population, whose formation is *related* to each other.

Statistically, however, it is still reasonable to assume that SNe with more massive progenitors will have a higher probability to be associated with younger stellar populations in their environments (and vice versa, since the targets were uniformly selected, observed, and analysed). Following this assumption, we discuss the environments and progenitors for the SESN types in the following subsections.

3.1 Types IIb, Ib, and Ic

Fig. 8 compares the cumulative age distributions for the youngest stellar populations detected in the types IIb, Ib, and Ic SN environments. The distributions are very similar between Type IIb and Type Ib SNe, while that for Type Ic SNe is systematically much younger. We performed a two-sample Anderson–Darling test[9] between Type Ic and types IIb + Ib; the null hypothesis that the two samples are drawn from the same distribution can be rejected at a 6 per cent significance level. The median log ages of the detected youngest populations are $\log(t/\mathrm{yr}) = 6.62 \pm 0.03$ for Type Ic SNe and 6.78 ± 0.02 for types Ib + IIb SNe. This suggests that the Type Ic SN progenitors are on average younger and more massive than those of Type IIb and Type Ib SNe, while the Type IIb and Type Ib SNe have on average indistinguishable progenitor masses.

In the upper panel of Fig. 8, the age uncertainties are propagated only from the photometric uncertainties. As mentioned in Section 2.3.2, however, there could be other error sources not included in our population fitting. While the interacting binaries and ambiguous star clusters may lead to an age underestimation, their effects are similar for different SN types since our analysis is performed in a uniform way. For the other error sources (distances, extinction law, small-number statistics, etc.), we conservatively assume that they contribute an additional uncertainty of 0.05 dex to the age determination (see the discussion in Section 2.3.2). The updated age distributions are displayed in the lower panel of Fig. 8; while the distributions become broader, the difference between Type Ic and types IIb + Ib SNe is still significant. The uncertainties of the median log ages increase by 0.01 dex.

[9]Unlike the Kolmogorov–Smirnov test, which uses only the supremum distance between two cumulative distribution functions (CDFs), the Anderson–Darling test uses the sum of all squared distances between two CDFs to test the null hypothesis; therefore, it is more sensitive to CDF differences in the tails.

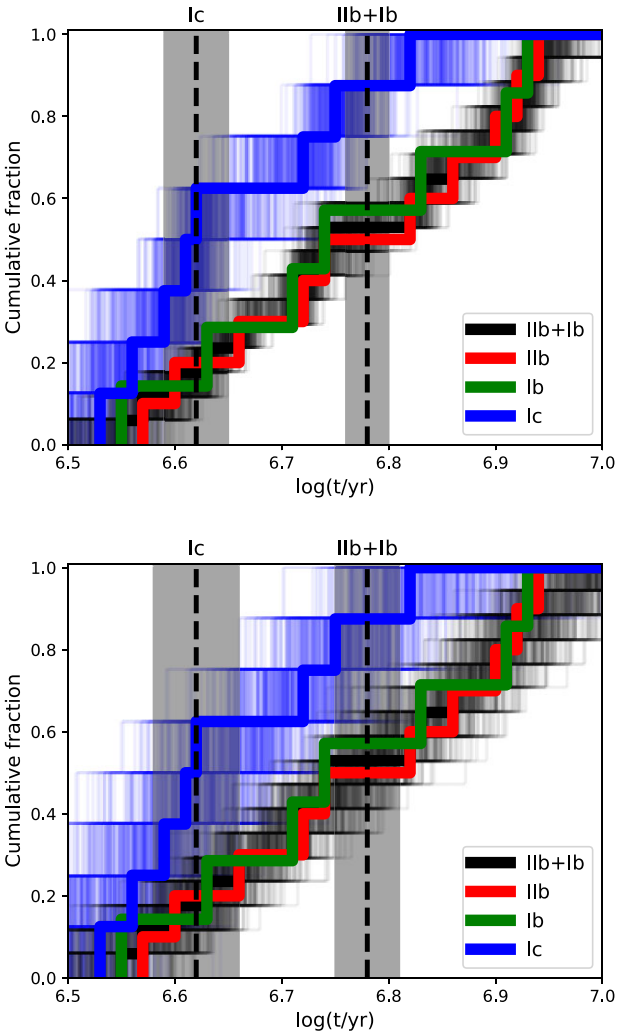

Figure 8. Cumulative age distributions of the detected youngest stellar populations in the types IIb (red), Ib (green), and Ic (blue) SN environments. The total cumulative age distribution for the combined sample of types IIb + Ib SNe is shown in black. The thinner lines are 500 random realizations derived from the age uncertainties; in the upper panel, the uncertainties are propagated from the photometric uncertainties, while in the lower panel, we conservatively assume an additional uncertainty of 0.05 dex from sources unaccounted for in our modelling (such as distance, extinction law, small-number statistics, etc.). The median log ages are shown by the vertical dashed lines with the shaded regions reflecting their uncertainties.

We also use an alternative method without isochrone fitting to qualitatively check the environmental difference for the different SN types; if the Type Ic SNe tend to be associated with younger stellar populations, their environments will have a larger number of bright stars than the Type IIb and Type Ib SNe. We calculate the absolute magnitudes of the surrounding stellar populations and correct their Galactic extinctions; apart from a few SNe with large distances and/or high extinctions (Type IIb SN 2010as, SN 2015Y, and SN2016bas; Type Ib SN 2016cdd; and Type Ic SN 2005aw), the detections are complete down to limits of $m_{F300X} = -7.5$ mag and $m_{F475X} = -6.5$ mag. The Type IIb SN 2009dq is also excluded since its environment contains many sources that are too bright to be single/binary stars but are more likely to be star clusters (Fig. 1). We find that the types IIb/Ib/Ic SN environments have on average 5/8/15 stars brighter than $m_{F300X} = -7.5$ mag, and 7/5/17 stars brighter than

$m_{F475X} = -6.5$ mag, respectively. This is consistent with the previous finding that Type Ic SN environments are on average younger than the Type IIb and Type Ib SNe. In this analysis, we have not corrected for the internal extinctions within the host galaxies, but the stellar population fitting shows that Type Ic SNe tend to have higher internal extinctions than the Type IIb and Type Ib SNe (Table 2), so the number of bright stars could potentially be even larger for the Type Ic SNe. All these results suggest that the Type Ic SN environments and progenitors are significantly different from those of Type IIb and Type Ib SNe.

3.1.1 A hybrid envelope-stripping mechanism?

Fang et al. (2019) analysed the late-time nebular spectra of 13 Type IIb, 16 Type Ib, and 16 Type Ic SNe. They found that Type Ic SNe have larger [O I]/[Ca II] line ratios than Type IIb and Type Ib SNe, while those for Type IIb and Type Ib SNe are very similar to each other. This result is later justified by their more recent work (Fang et al. 2022) based on a larger sample. The [O I]/[Ca II] line ratio is a good indicator of the final carbon–oxygen core mass, which is higher for more massive SN progenitors. Therefore, they have reached the same conclusion as we draw from the above environmental analysis.

Our result therefore supports the hybrid envelope-stripping model proposed by Fang et al. (2019, see also the schematic diagram in Fig. 9) for the origins of SESNe. The indistinguishable progenitor masses between Type IIb and Type Ib SNe suggest that the hydrogen envelope is stripped by a mass-insensitive process, and binary interaction is the best candidate without major difficulties. The outcome of binary interaction is strongly dependent on the initial binary separation: a star in a relatively wide binary may end up with a small residual hydrogen envelope and explode as a Type IIb SN, while a star of the same initial mass in a closer binary can completely lose its hydrogen envelope and explode as a Type Ib SN (e.g. Claeys et al. 2011). The effect of binary interaction depends weakly on the progenitor mass, and we note that a mass- and metallicity-dependent stellar wind may remove the residual hydrogen envelope left after the binary interaction (e.g. Yoon, Dessart & Clocchiatti 2017).

The fact that Type Ic SNe appear to favour higher progenitor masses than Type IIb and Type Ib SNe suggests that the stripping of the helium envelope is caused by a mass-sensitive process. This may be the stellar wind of the hydrogen-poor progenitor in the post-binary interaction phase, which is stronger for more massive stars (Vink 2017; note that binary interaction alone is very difficult to remove the entire helium envelope in self-consistent models; Benvenuto & Bersten 2017). It is also possible that a very massive progenitor can lose all of its hydrogen- and helium-rich layers solely via its own stellar wind without the aid of binary interaction. Some Type Ic SNe may still have modest He envelopes that are not completely stripped, but their helium lines are not excited due to, e.g. the weak mixing between helium and radioactive elements (Dessart et al. 2012).

The differences between types IIb + Ib and Type Ic SN progenitors found by Fang et al. (2019) and this work are only *statistically* meaningful instead of being specific about individual progenitors. It is possible that a Type IIb or Type Ib SN progenitor could be more massive than that for a Type Ic SN. Similarly, the proposed hybrid envelope-stripping model may just account for most, instead of all, of the observed SN populations, and there could be many other progenitor channels for the origins of SESNe (e.g. Yoon 2017; Yoon et al. 2017; Hirai et al. 2020).

3.1.2 Comparison with previous works

The environments of SESNe have been studied in a number of previous works with a variety of methods. For example, Galbany et al. (2018) and Kuncarayakti et al. (2018) used the Hα equivalent width to estimate the ages of the ionizing stellar populations, and Anderson et al. (2012) and Kangas et al. (2013) analysed the SN spatial correlation with Hα emission (and other tracers of star formation). Kangas et al. (2013) showed that Type Ic SNe are most strongly correlated with recent star formation, while the difference between Type II and Type Ib SNe is insignificant (consistent with our results). On the other hand, however, some of the works found a trend that, following types IIb $\rightarrow$ Ib $\rightarrow$ Ic, the SNe occur in progressively younger environments (e.g. Anderson et al. 2012; Kuncarayakti et al. 2018).

We caution that the use of the Hα equivalent width as a stellar age indicator may suffer from large uncertainties. Its value is very sensitive to the covering factor, the older stellar populations along the same line of sight (which contribute to the stellar continuum), and whether the effect of interacting binaries is taken into account. Recent works (e.g. Xiao, Stanway & Eldridge 2018; Schady et al. 2019; Xiao et al. 2019) found that the derived stellar ages can be very different if these effects were or were not considered; Sun et al. (2021) showed that accurate stellar ages can only be obtained by a detailed photoionization calculation and a full modelling of the nebular spectral lines. Large uncertainties may also affect the spatial correlation analysis. As pointed out by Crowther (2013), the giant H II regions (rather than isolated and compact ones) in the vicinity of most SN sites can undergo complicated and multigeneration evolution, and the observed spatial association provides only weak constraints on the SN progenitor masses. Moreover, some SNe apparently associated with H II regions on the low-spatial resolution images may actually have an offset between each other (e.g. Maund & Ramirez-Ruiz 2016).

Studying the resolved stellar populations allows a direct age estimate of the SN environments. Maund (2018) analysed 23 SESNe and found that the characteristic ages for the environmental populations (approximately the mean ages for all the detected populations for a given SN type, not just the youngest population in the environment) are $\log(t/\mathrm{yr}) = 7.20$, 7.05, and 6.57 for types IIb, Ib, and Ic SNe, respectively. However, that work was based on a heterogeneous data set and the effect of selection bias is very difficult to estimate. In addition, many of the analysed SNe lack UV observations; since the optical colour is very insensitive to stellar age, the age determination may therefore have relatively large uncertainties, especially for the youngest populations of only a few Myrs.

In our analysis, the age distributions of the youngest environmental populations are almost identical for the Type IIb and Type Ib SNe (Fig. 8). We cannot rule out the possibility that this is due to the measurement uncertainties and/or the limited sample size. Observations of larger samples are required to further confirm this result.

3.2 Type Ibn

Type Ibn SNe are those that exhibit narrow helium lines with little evidence for hydrogen. The narrow helium lines are a signature of strong interaction between the SN ejecta and helium-rich CSM. The CSM was formed via eruptive mass-loss of their progenitors shortly before their explosions (Smith 2017). Early studies proposed that their progenitors are massive WR stars stripped by their powerful winds (e.g. Foley et al. 2007; Pastorello et al. 2007). More recently,

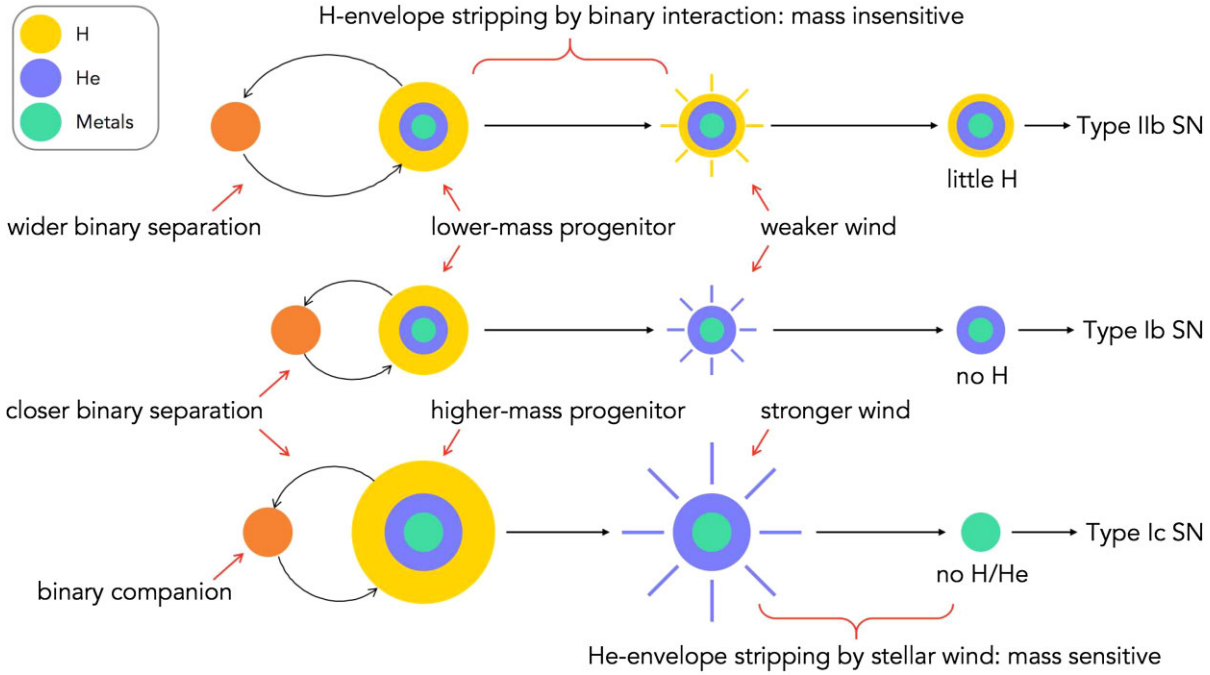

Figure 9. A hybrid envelope-stripping mechanism that dominates the origins of types IIb, Ib, and Ic SNe.

Shivvers et al. (2017b) ruled out a WR progenitor for SN 2015G by examining its pre-explosion images. Sun et al. (2020a) found a progenitor initial mass of only $\lesssim$12 $M_\odot$ for SN 2006jc by analysing its surviving binary companion. Modelling of the SN spectra (Dessart, Hillier & Kuncarayakti 2022) showed that Type Ibn SN progenitors have final masses of only $\lesssim$5 $M_\odot$, much lower than those for WR stars.

For the Type Ibn SN 2006jc and SN 2015G, our deep imaging did not detect any obvious stellar populations in their environments younger than $\log(t/\mathrm{yr}) = 7.3$ and 7.2, respectively (Table 2 and Fig. 7). The age limits were derived by assuming zero internal extinctions within their host galaxies. If we adopt the extinction estimates by Pastorello et al. (2007) and Shivvers et al. (2017b), the age limit changes to $\log(t/\mathrm{yr}) = 7.1$ for SN 2015G, while that for SN 2006jc is almost unchanged. The age limits correspond to progenitor masses of $M_{\rm ini} \lesssim 11.9$ $M_\odot$ for SN 2006jc and $M_{\rm ini} \lesssim 13.8$ $M_\odot$ (assuming zero internal extinction) or 16.3 $M_\odot$ (using the extinction estimate from Shivvers et al. 2017b) for SN 2015G. These constraints argue against massive WR progenitors, whose lifetimes are only a few Myrs.[10] Their progenitors are most likely stripped via binary interaction, which then underwent eruptive mass-loss shortly before their core collapse. These two processes led to the stripping of their hydrogen envelopes and the formation of the dense helium-rich CSM. Therefore, this result confirms that violent eruptions, often seen in very massive (>25–30 $M_\odot$) luminous blue variables, can also occur in much lower mass stars stripped in binaries (Fuller & Ro 2018; Wu & Fuller 2022; see also Sun et al. 2020a, for a detailed discussion).

For the more distant SN 2015U, the age limit [$\log(t/\mathrm{yr}) > 6.9$] is not sufficient to robustly reject a WR progenitor. This limit is likely to be overestimated since we assumed zero internal extinction, but SN 2015U seems to be in a dusty area. Moreover, there is a UV blob in its vicinity, which could be an unresolved young star-forming complex. Therefore, the environment of SN 2015U is rather ambiguous.

3.3 Type Ic-BL

Type Ic-BL SNe are characterized by the broad lines in their spectra, indicating extremely fast expansion velocities. Their explosion energies can reach $\sim 10^{52}$ erg, almost an order of magnitude higher than the normal core-collapse SNe. Lyman et al. (2016) found relatively low ejecta masses for almost all Type Ic-BL SNe in their sample, suggesting moderately massive progenitors of $M_{\rm init} = 8$–20 $M_\odot$ stripped in binaries. In contrast, Taddia et al. (2019) showed that at least 21 per cent of the Type Ic-BL SNe have very large ejecta masses of >5.5 $M_\odot$ and should arise from the more massive WR progenitors with $M_{\rm ini} > 28$ $M_\odot$.

In our sample, the Type Ic-BL SN 1997dq was poorly studied previously (see, however, Mazzali et al. 2004) and SN 2002ap has received far more attention. For SN 2002ap, the light-curve analysis of Mazzali et al. (2002) derived a carbon–oxygen core mass of 5 $M_\odot$, corresponding to an initial mass of 20–25 $M_\odot$ for the progenitor. Crockett et al. (2007) ruled out any single progenitors that have not evolved into a WR phase based on detection limits on the pre-explosion images; they suggested that the progenitor, if it were indeed a single star, should have an initial mass of at least 30–40 $M_\odot$ and a higher-than-standard mass-loss rate. More recently, Zapartas et al. (2017) constrained the progenitor initial mass to be $\lesssim$23 $M_\odot$ with binary population synthesis.

Maund (2018) detected only a few stars in the environment of SN 2002ap based on optical images acquired by the High Resolution

[10]Recently, Beasor et al. (2021) derived an older age of $\sim$10 Myr for the Galactic cluster Westerlund 1, which hosts dozens of WR stars, from its cool supergiant population. If the WR stars have the same age as the cool supergiants, the age and initial mass limits for WR stars may have to be softened to some extent, possibly owing to their binary evolutionary channel. However, we also note that Westerlund 1 was formed in an extended period of star formation of several Myrs, so the WR stars in this cluster may still have very young ages consistent with previous constraints (Crowther 2007).

Channel of *HST*'s Advanced Camera for Surveys. Our new images, which use the extremely wide *F300X* and *F475X* filters and reach deeper detection limits, clearly reveal a young and resolved stellar population in the vicinity of SN 2002ap (Fig. 6). This is consistent with the deep UV images acquired by Zapartas et al. (2017, their fig. 1) in the *F275W* and *F336W* filters with exposure times of 2778 s in each band. The derived age [$\log(t/\mathrm{yr}) = 6.96^{+0.04}_{-0.05}$] corresponds to a progenitor initial mass ($M_{\rm ini}$) of $21.6^{+2.5}_{-1.8}$ $\mathrm{M}_{\odot}$, assuming that the progenitor is a member of and has the same age as the detected population. This value is consistent with the previous estimates as mentioned earlier. For SN 1997dq, the detected environmental population suggests a progenitor mass ($M_{\rm ini}$) of $22.5^{+2.8}_{-2.3}$ $\mathrm{M}_{\odot}$, very similar to that of SN 2002ap. It is also possible, however, that the progenitor may have a lower initial mass if it belongs to an undetected older stellar population. These results are inconsistent with massive WR progenitors and agree with a binary progenitor channel (but the envelope stripping may still be aided by its own stellar wind). Note that Type Ic-BL SNe prefer low-metallicity environments (Modjaz et al. 2020), where stars have weaker winds and the initial mass threshold can be as high as $\sim$30 $\mathrm{M}_{\odot}$ for a single star to evolve into the WR phase (Crowther 2007).

4 SUMMARY AND CONCLUSIONS

This paper reports an environmental analysis of 41 SESNe. The targets were selected and observed uniformly and unbiasedly, and deep UV–optical imaging was conducted by the *HST* to probe the young stars in the SN environments. We used a hierarchical Bayesian approach to fit resolved stellar populations on the CMDs in order to derive their ages and extinctions. The high sensitivity of UV–optical colour to stellar age/extinction allows us to make very precise measurements, with typical uncertainties smaller than 0.1 dex in log age and 0.1 mag in extinction in most cases.

As many as 80 per cent of the observed types IIb, Ib, and Ic SNe have stellar populations younger than 10 Myr in their environments. The age distributions for the youngest environmental populations for Type IIb and Type Ib SNe are very similar to each other, while that for Type Ic SNe is systematically much younger. This suggests that Type Ic SNe have more massive progenitors than Type IIb and Type Ib SNe; in contrast, no compelling evidence is found for any significant difference between Type IIb and Type Ib SN progenitor masses.

This result supports a hybrid model of envelope stripping for the origins of SESNe (as proposed by Fang et al. 2019). In this scenario, the stripping of the hydrogen envelope is mostly caused by binary interaction as a mass-insensitive process, while that for the helium envelope could be due to a mass-sensitive mechanism, such as the wind of the hydrogen-poor progenitor at the post-binary interaction phase.

For the Type Ibn SNe, our deep imaging excludes any young stellar populations in the environments of SN 2006jc and SN 2015G that correspond to massive WR progenitors. They most likely arise from moderately massive ($\lesssim$11.9 and $\lesssim$16.3 $\mathrm{M}_{\odot}$, respectively) stars stripped in interacting binaries. For the more distant SN 2015U, however, the age limit is not sufficient to make any useful constraints. This result confirms that the very violent eruptions, often seen in the very massive luminous blue variables, can also occur in much lower mass stars stripped in binaries, forming dense and helium-rich CSM shortly before their final explosion.

For the Type Ic-BL SNe, we detect young stellar populations in the vicinity of both SN 1997dq and SN 2002ap. Their progenitors would have initial masses ($M_{\rm ini}$) of $22.5^{+2.8}_{-2.3}$ and $21.6^{+2.5}_{-1.8}$ $\mathrm{M}_{\odot}$, respectively, if they are coeval with the detected populations. This result also argues against WR progenitors for both SNe and favours an interacting binary progenitor channel possibly aided by their own stellar winds.

ACKNOWLEDGEMENTS

The authors are very grateful to Prof. Keiichi Maeda, Mr Qiliang Fang, and the anonymous referee for their very helpful comments on this paper. Research of N-CS, JRM, and PAC is funded by the Science and Technology Facilities Council through grant ST/V000853/1. This paper is based on observations made with the NASA/ESA *Hubble Space Telescope*.

DATA AVAILABILITY

Data used in this work are all publicly available from the Mikulski Archive for Space Telescope (https://archive.stsci.edu).

REFERENCES

Aldering G., Humphreys R. M., Richmond M., 1994, AJ, 107, 662
Anderson J. P., Habergham S. M., James P. A., Hamuy M., 2012, MNRAS, 424, 1372
Beasor E. R., Davies B., Smith N., Gehrz R. D., Figer D. F., 2021, ApJ, 912, 16
Benvenuto O. G., Bersten M. C., 2017, in Alsabti A. W., Murdin P., eds, Handbook of Supernovae. Springer Int. Publ. AG, Cham, p. 649
Beswick R. J., Fenech D., Thrall H., Argo M. K., Muxlow T. W. B., Pedlar A., 2005, IAU Circ., 8572, 1
Bressan A., Marigo P., Girardi L., Salas nich B., Dal Cero C., Rubele S., Nanni A., 2012, MNRAS, 427, 127
Cao Y. et al., 2013, ApJ, 775, L7
Childress M., Scalzo R., Yuan F., Zhang B., Ruiter A., Seitenzahl I., Schmidt B., Tucker B., 2015, Astron. Telegram, 7368, 1
Chornock R., Berger E., 2009, Cent. Bur. Electron. Telegrams, 2086, 1
Chornock R., Filippenko A. V., 2001, IAU Circ., 7577, 1
Claeys J. S. W., de Mink S. E., Pols O. R., Eldridge J. J., Baes M., 2011, A&A, 528, A131
Crockett R. M. et al., 2007, MNRAS, 381, 835
Crockett R. M. et al., 2008, MNRAS, 391, L5
Crowther P. A., 2007, ARA&A, 45, 177
Crowther P. A., 2013, MNRAS, 428, 1927
della Valle M., Pasquini L., Phillips M., McCarthy P., 1990, IAU Circ., 5079, 1
Dessart L., Hillier D. J., Li C., Woosley S., 2012, MNRAS, 424, 2139
Dessart L., Hillier D. J., Kuncarayakti H., 2022, A&A, 658, A130
Dolphin A. E., 2000, PASP, 112, 1383
Drout M. R. et al., 2016, ApJ, 821, 57
Efremov Y. N., 1995, AJ, 110, 2757
Eldridge J. J., Fraser M., Maund J. R., Smartt S. J., 2015, MNRAS, 446, 2689
Fang Q., Maeda K., Kuncarayakti H., Sun F., Gal-Yam A., 2019, Nat. Astron., 3, 434
Fang Q. et al., 2022, ApJ, 928, 151
Filippenko A. V., Chornock R., 2000, IAU Circ., 7511, 1
Filippenko A. V., Chornock R., 2001, IAU Circ., 7638, 1
Filippenko A. V., Foley R. J., 2005, IAU Circ., 8486, 1
Filippenko A. V., Korth S., 1991, IAU Circ., 5234, 1
Filippenko A. V., McCarthy P., 1990, IAU Circ., 5090, 1
Filippenko A. V., Chornock R., Modjaz M., 2000, IAU Circ., 7547, 1
Fitzpatrick E. L., 2004, in Witt A. N., Clayton G. C., Draine B. T., eds, ASP Conf. Ser. Vol. 309, Astrophysics of Dust. Astron. Soc. Pac., San Francisco, p. 33
Folatelli G. et al., 2014, ApJ, 792, 7
Foley R. J., 2009, Cent. Bur. Electron. Telegrams, 1858, 1

Foley R. J., Wong D. S., Ganeshalingam M., Filippenko A. V., Chornock R., 2004, IAU Circ., 8339, 1
Foley R. J., Smith N., Ganeshalingam M., Li W., Chornock R., Filippenko A. V., 2007, ApJ, 657, L105
Foley R. J. et al., 2009, AJ, 138, 376
Fox O. D. et al., 2022, ApJ, 929, L15
Fuller J., Ro S., 2018, MNRAS, 476, 1853
Gagliano A. et al., 2022, ApJ, 924, 55
Galbany L. et al., 2018, ApJ, 855, 107
Green D. W. E., 2009a, Cent. Bur. Electron. Telegrams, 1789, 1
Green D. W. E., 2009b, Cent. Bur. Electron. Telegrams, 1807, 1
Hamuy M. et al., 2009, ApJ, 703, 1612
Heger A., Fryer C. L., Woosley S. E., Langer N., Hartmann D. H., 2003, ApJ, 591, 288
Hirai R., Sato T., Podsiadlowski P., Vigna-Gómez A., Mandel I., 2020, MNRAS, 499, 1154
Hosseinzadeh G., Arcavi I., Howell D. A., McCully C., Valenti S., 2016a, Astron. Telegram, 8814, 1
Hosseinzadeh G., Arcavi I., Howell D. A., McCully C., Valenti S., 2016b, Astron. Telegram, 9065, 1
Itagaki K., Noguchi T., Nakano S., Yusa T., Wang X.-F., Liu Q., Zhang J.-J., Zhang T.-M., 2012, Cent. Bur. Electron. Telegrams, 3148, 1
Jeffreys H., 1961, Theory of Probability, 3rd edn. Oxford Univ. Press, Oxford
Kangas T., Mattila S., Kankare E., Kotilainen J. K., Väisänen P., Greimel R., Takalo A., 2013, MNRAS, 436, 3464
Kankare E. et al., 2014, A&A, 572, A75
Kilpatrick C. D. et al., 2017, MNRAS, 465, 4650
Kilpatrick C. D. et al., 2021, MNRAS, 504, 2073
Kim M. et al., 2014, Cent. Bur. Electron. Telegrams, 3777, 1
Kinugasa K. et al., 2002, ApJ, 577, L97
Koenig X. P., Allen L. E., Gutermuth R. A., Hora J. L., Brunt C. M., Muzerolle J., 2008, ApJ, 688, 1142
Kuncarayakti H. et al., 2018, A&A, 613, A35
Lane D. J., Gray P., Fillipenko A. V., Barth A. J., 1995, IAU Circ., 6138, 1
Leloudas G. et al., 2012, A&A, 541, A129
Lyman J. D., Bersier D., James P. A., Mazzali P. A., Eldridge J. J., Fraser M., Pian E., 2016, MNRAS, 457, 328
Makarov D., Prugniel P., Terekhova N., Courtois H., Vauglin I., 2014, A&A, 570, A13
Martins F., Palacios A., 2013, A&A, 560, A16
Matheson T., Challis P., Kirshner R., Berlind P., 2004b, IAU Circ., 8304, 1
Maund J. R., 2017, MNRAS, 469, 2202
Maund J. R., 2018, MNRAS, 476, 2629
Maund J. R., 2019, ApJ, 883, 86
Maund J. R., Ramirez-Ruiz E., 2016, MNRAS, 456, 3175
Maund J. R., Smartt S. J., Kudritzki R. P., Podsiadlowski P., Gilmore G. F., 2004, Nature, 427, 129
Maund J. R. et al., 2011, ApJ, 739, L37
Maund J. R., Pastorello A., Mattila S., Itagaki K., Boles T., 2016, ApJ, 833, 128
Mazzali P. A. et al., 2002, ApJ, 572, L61
Mazzali P. A., Deng J., Maeda K., Nomoto K., Filippenko A. V., Matheson T., 2004, ApJ, 614, 858
Mazzali P. A., Deng J., Hamuy M., Nomoto K., 2009, ApJ, 703, 1624
Milisavljevic D., Fesen R., Soderberg A., Pickering T., Kotze P., 2011, Cent. Bur. Electron. Telegrams, 2902, 1
Milisavljevic D. et al., 2015, ApJ, 815, 120
Miller A. E. et al., 2022, MNRAS, 512, 1196
Modjaz M. et al., 2020, ApJ, 892, 153
Monard L. A. G. et al., 2014, Cent. Bur. Electron. Telegrams, 3977, 1
Morrell N., Hamuy M., Folatelli G., Roth M., 2005, IAU Circ., 8507, 1
Nakano S. et al., 2012, Cent. Bur. Electron. Telegrams, 3263, 1
Navasardyan H., Benetti S., 2009, Cent. Bur. Electron. Telegrams, 1806, 1
Navasardyan H., Benetti S., Harutyunyan A., Agnoletto I., Bufano F., Cappellaro E., Turatto M., 2008, Cent. Bur. Electron. Telegrams, 1325, 1
Pastorello A. et al., 2007, Nature, 447, 829
Podsiadlowski P., Joss P. C., Hsu J. J. L., 1992, ApJ, 391, 246
Qiu Y., Li W., Qiao Q., Hu J., 1999, AJ, 117, 736
Quimby R. et al., 2004, IAU Circ., 8446, 1
Richardson C. J., Zanolin M., Andresen H., Szczepańczyk M. J., Gill K., Wongwathanarat A., 2022, Phys. Rev. D, 105, 103008
Ryder S. D. et al., 2018, ApJ, 856, 83
Salpeter E. E., 1955, ApJ, 121, 161
Schady P., Eldridge J. J., Anderson J., Chen T.-W., Galbany L., Kuncarayakti H., Xiao L., 2019, MNRAS, 490, 4515
Schlafly E. F., Finkbeiner D. P., 2011, ApJ, 737, 103
Schmidt B., Salvo M., 2005, IAU Circ., 8496, 1
Schneider F. R. N., Izzard R. G., Langer N., de Mink S. E., 2015, ApJ, 805, 20
Shivvers I. et al., 2016, MNRAS, 461, 3057
Shivvers I. et al., 2017a, PASP, 129, 054201
Shivvers I. et al., 2017b, MNRAS, 471, 4381
Smartt S. J., 2009, ARA&A, 47, 63
Smith N., 2014, ARA&A, 52, 487
Smith N., 2017, in Alsabti A. W., Murdin P., eds, Handbook of Supernovae. Springer Int. Publ. AG, Cham, p.403
Sollerman J., Leibundgut B., Spyromilio J., 1998, A&A, 337, 207
Sun N.-C. et al., 2017a, ApJ, 835, 171
Sun N.-C. et al., 2017b, ApJ, 849, 149
Sun N.-C. et al., 2018, ApJ, 858, 31
Sun N.-C., Maund J. R., Hirai R., Crowther P. A., Podsiadlowski P., 2020a, MNRAS, 491, 6000
Sun N.-C., Maund J. R., Crowther P. A., 2020b, MNRAS, 497, 5118
Sun N.-C., Maund J. R., Crowther P. A., Fang X., Zapartas E., 2021, MNRAS, 504, 2253
Sun N.-C. et al., 2022, MNRAS, 510, 3701
Taddia F. et al., 2019, A&A, 621, A71
Tartaglia L. et al., 2017, ApJ, 836, L12
Taubenberger S., Pastorello A., Benetti S., Aceituno J., 2005, IAU Circ., 8474, 1
Tully R. B. et al., 2013, AJ, 146, 86
Tully R. B., Courtois H. M., Sorce J. G., 2016, AJ, 152, 50
Van Dyk S. D. et al., 2014, AJ, 147, 37
Van Dyk S. D. et al., 2018, ApJ, 860, 90
Vink J. S., 2017, A&A, 607, L8
Wiggins P. et al., 2015, Cent. Bur. Electron. Telegrams, 4128, 1
Williams B. F., Hillis T. J., Blair W. P., Long K. S., Murphy J. W., Dolphin A., Khan R., Dalcanton J. J., 2019, ApJ, 881, 54
Wu S. C., Fuller J., 2022, ApJ, 930, 119
Xiang D. et al., 2019, ApJ, 871, 176
Xiao L., Stanway E. R., Eldridge J. J., 2018, MNRAS, 477, 904
Xiao L., Galbany L., Eldridge J. J., Stanway E. R., 2019, MNRAS, 482, 384
Yoon S.-C., 2017, MNRAS, 470, 3970
Yoon S.-C., Dessart L., Clocchiatti A., 2017, ApJ, 840, 10
Zapartas E. et al., 2017, ApJ, 842, 125

This paper has been typeset from a TEX/LATEX file prepared by the author.